Elucidating the role of charge density on the growth of CaCO3 crystals underneath Calix[4]arene monolayers

Dirk Volkmer, Marc Fricke, Michael Gleiche, Lifeng Chi

Angaben zur Veröffentlichung / Publication details:

Volkmer, Dirk, Marc Fricke, Michael Gleiche, and Lifeng Chi. 2005. "Elucidating the role of charge density on the growth of CaCO3 crystals underneath Calix[4]arene monolayers." *Materials Science and Engineering: C* 25 (2): 161–67. https://doi.org/10.1016/j.msec.2005.01.006.

Elucidating the role of charge density on the growth of $CaCO_3$ crystals underneath Calix[4]arene monolayers

Dirk Volkmer[a,*], Marc Fricke[b], Michael Gleiche[c], Lifeng Chi[c]

[a]*Department of Inorganic Chemistry II, University of Ulm, D-89081 Ulm, Albert-Einstein-Allee II, Germany*
[b]*Faculty of Chemistry (AC1), University of Bielefeld, D-33501 Bielefeld, P.O. Box 100 131, Germany*
[c]*Faculty of Physics (Interface Physics), University of Münster, Germany*

1. Introduction

Crystallization of inorganic solids at the surfaces of biological tissues is an important step in biomineralization [1]. However, the natural processes that control the formation of a particular crystal polymorph or morphology yet are poorly understood. Artificial matrices such as Langmuir monolayers [2], self-assembled monolayers (SAMs) [3] and polymer thin films [4] have been employed in order to gain insights into the putative mechanisms of template-directed mineralization. Physicochemical parameters such as interfacial electrostatics [5], hydrogen bonding [3,5] and interfacial molecular recognition events including geometrical lattice matching [2,6] and stereochemical complementarity [3,7] are considered crucial factors in this context. More recently, kinetic effects were discussed on the basis of in situ grazing incidence X-ray diffraction experiments [8]. However, few studies have attempted to quantify the influence of electrostatic interactions on heterogeneous crystal nucleation employing suitable model systems such as Langmuir monolayers [9].

In our previous work we have reported on calcite single crystals growing underneath monolayers of tetracarboxy-calix[4]arenes (**2**) [10] and tetracarboxy-resorc[4]arenes (**3**) (Scheme 1) [11]. Monolayers of **2** and **3** both lead to formation of the same truncated calcite single crystals with their {01.2} crystal face attaching to the monolayer. Detailed investigations on the structures of **2** and **3** have shown that their supramolecular packing arrangements are quite different and thus a heteroepitaxial correlation between the charged headgroups of the monolayer and the (polar) $CaCO_3$ crystal face that attaches to the monolayer can be ruled out.

We have therefore suggested that macroscopic monolayer properties such as average charge density or mean dipole moment of the templating monolayer determine the orientation of $CaCO_3$ crystals [10,11]. In order to gain more insights into the interactions between dipolar monolayers and hydrated calcium and carbonate ions we now employ the non-charged amphiphilic 5,11,17,23-tetrakis-(1,1,3,3-tetramethylbutyl)-25,26,27,28-tetra(2-hydroxyethoxy)calix[4]arene (**1**), the monolayer of which strongly inhibits

* Corresponding author. Tel.: +49 731 50 23921; fax: +49 731 50 23039.
E-mail address: dirk.volkmer@chemie.uni-ulm.de (D. Volkmer).

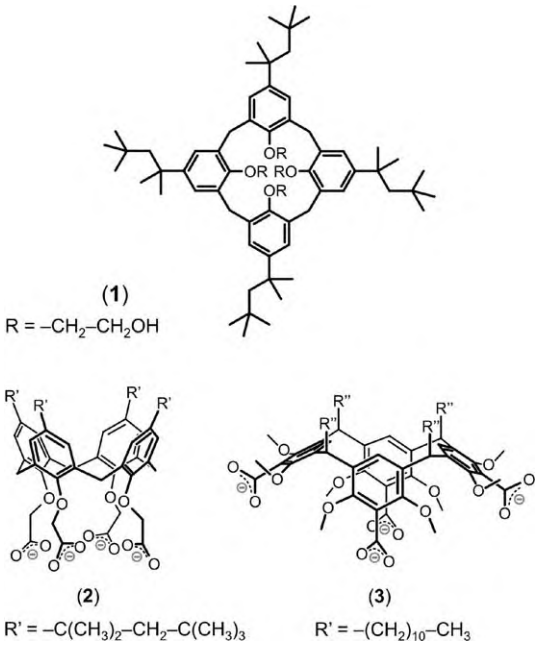

Scheme 1. Amphiphilic compounds used in the present and in previous investigations: 5,11,17,23-tetrakis-(1,1,3,3-tetramethylbutyl)-25,26,27,28-tetra(2-hydroxyethoxy)calix[4]arene (**1**), 5,11,17,23-tetrakis-(1,1,3,3-tetramethylbutyl)-25,26,27,28-tetra(carboxymethoxy)calix[4]arene (**2**), and *rccc*-5,11,17,23-tetracarboxy-4,6,10,12,16,18,22,24-octa-*O*-methyl-2,8,14,20-tetra(*n*-undecyl)resorc[4]arene (**3**).

heterogeneous nucleation of $CaCO_3$ crystals. Monolayers of **1** and **2** were spread on aqueous subphases of different compositions and the resulting surface pressure–area (π–A) isotherms are analysed in terms of phase behaviour. The simultaneously recorded surface potential–area (ΔV–A) isotherms reveal insights into the interactions between subphase ions and monolayer molecules. The monolayer structure of compound **1** is furthermore characterized by means of Brewster angle microscopy (BAM). The growth of calcite ($CaCO_3$) single crystals underneath monolayers of **1** and **2** is monitored in situ by optical microscopy.

2. Results and discussion

2.1. Monolayer studies

Langmuir monolayers were formed on aqueous subphases by spreading compound **1** from trichloromethane/methanol (9:1) and **2** from trichloromethane solution using a Langmuir trough (NIMA 601BAM). The recorded surface pressure–area (π–A) isotherm provides information about monolayer stability and phase behaviour. The surface potential–area (ΔV–A) isotherm characterizes the pressure-dependent electrostatic properties of the monolayers. The measured surface potential attributes to the average orientation of amphiphilic (=dipolar) molecules in the monolayer. For monolayers built up from charged amphiphiles the solvation shell of water molecules, the first adlayer of counter ions, and the concentration gradient of ions perpendicular to the monolayer contribute to the surface potential, too [12].

Remarkably, the surface potential technique often allows to investigate monolayer properties at a very early stage of compression when the surface pressure still is at 0 mN/m. Fig. 1 shows the π–A and ΔV–A isotherms of compounds **1** and **2** spread on different aqueous subphases. Compound **1** forms relatively stable monolayers which collapse upon compression at a surface pressure of ~30 mN/m. The π–A isotherms gained from **1** on H_2O, and on 10 mM $CaCl_2$, respectively, are almost identical indicating a similar monolayer phase behaviour on both subphases. The onset of the pressure increase starts at a surface value in between 180 and 185 Å^2/molecule. The area per molecule of **1** in the monolayers is estimated from extrapolating the Langmuir isotherms toward zero pressure. The determined area values are listed in Table 1. The average area per molecule for compound **1** amounts to 170–180 Å^2 which is significantly (10–15%) larger than the corresponding value of the tetracarboxy-calix[4]arene (**2**). While the area per molecule (145–150 Å^2) of **2** as derived from the isotherm data have been shown previously to be in excellent agreement with the area value calculated from molecular packing analysis of X-ray structural data, the high surface area of **1** is hard to rationalize [10]. The single crystal X-ray structure analysis reveals a typical structure motif which consists of interdigitated close packed monolayers of **1** extending in the (1 −1 0) crystal plane, in contrast to the bilayer motif frequently reported for other amphiphilic calixarenes [13]. Due to interdigitation of cone shaped calix[4]arenes the molecular surface area in the most densely packed crystal lattice plane is rather small (144 Å^2/molecule). The larger surface area determined from the Langmuir isotherm thus indicates that compound **1** forms a regular monolayer at the air–water interface with the hydrophilic residues uniformly pointing towards the aqueous subphase. A similar behaviour has been observed for monolayers of the octaacid *rccc*-4,6,10,12,16,18,22,24-octakis-*O*-(carboxymethyl)-2,8,14,20-tetra(*n*-undecyl)resorc[4]arene (**4**) and the corresponding alcohol *rccc*-4,6,10,12,16,18,22,24-octa(2-hydroxyethoxy)-2,8,14,20-tetra(*n*-undecyl)resorc[4]arene (**5**) [14].

At a surface pressure of ~5 mN/m a temperature-dependent phase transition occurs which is reproducible (Fig. 1). At temperatures above 30 °C the kink disappears and the surface pressure increases linearly (not shown). It should be noted that the average area per molecule (145 Å^2) at the second kink at ~32 mN/m is in excellent agreement with the value derived from crystal structure analysis (144 Å^2) of **1** while the value is sufficiently large to rule out formation of a multilayer. Thus the first broad plateau which is found at a surface pressure >32 mN/m might indicate a second phase transition.

Temperature-dependent measurements support this interpretation: the π–A isotherms demonstrate that the surface pressure at which the plateau occurs decreases with increasing temperature. At a surface pressure >35 mN/m a

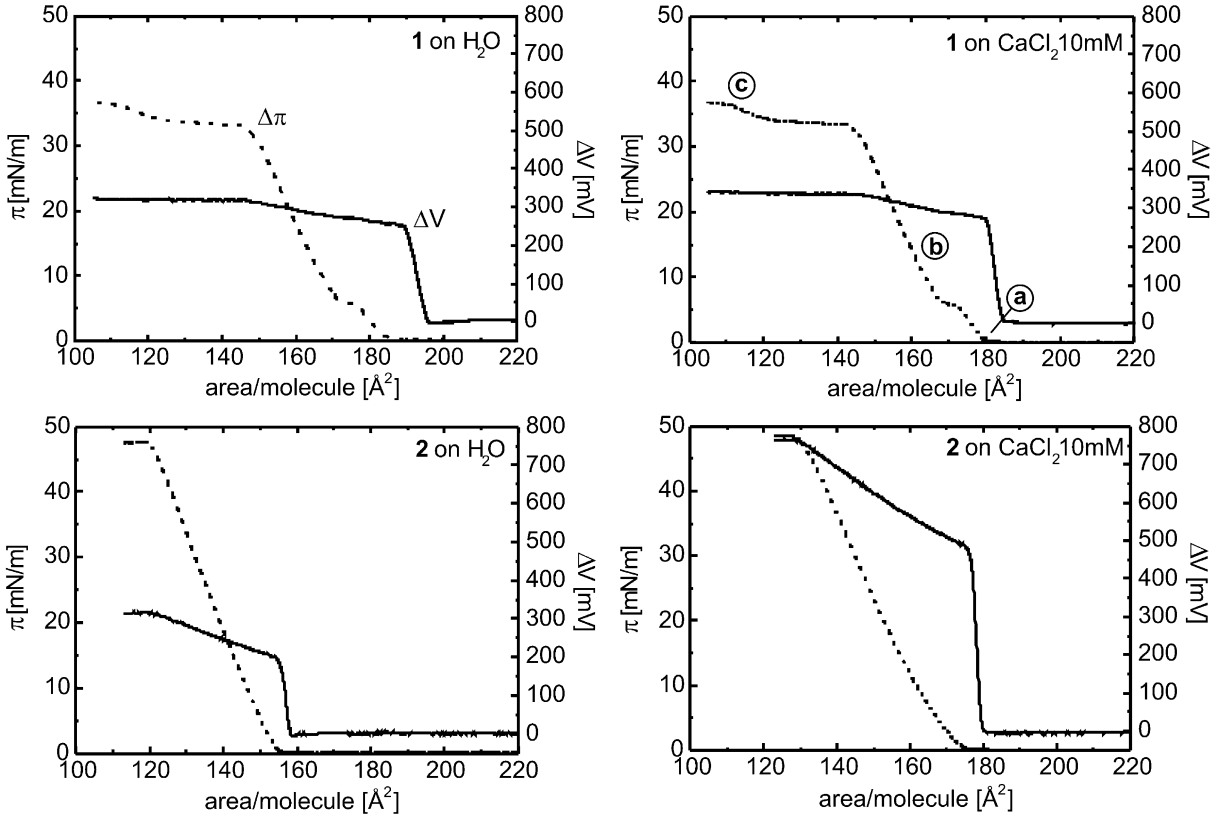

Fig. 1. From top row left to bottom row right: surface pressure–area, π–A (dashed line) and surface potential–area, ΔV–A (solid line) isotherms of **1** on H_2O (22 °C), **1** on $CaCl_2$ (c=10 mM, 22 °C; point markers a–c refer to the corresponding BAM images in Fig. 2), **2** on H_2O (22 °C), and **2** on $CaCl_2$ (c=10 mM, 22 °C).

second broad plateau occurs until the surface pressure increases again and the collapse pressure is reached at ~45 mN/m (not shown). A similar phase behaviour has been reported for monolayers of polyphenyl carboxylic acids [15]. However, a detailed analysis of the monolayer phase diagram of **1** is beyond the scope of this report.

BAM investigations corroborate that there is no difference in phase behaviour for monolayers of **1** spread on different subphases (H_2O and 10 mM $CaCl_2$). Fig. 2 shows a sequence of typical BAM images on $CaCl_2$ for selected pressure values. The BAM images show that at zero surface pressure a liquid-expanded phase forms (Fig. 2a). At 5 mN/m a liquid-condensed phase can be observed where the film appears homogeneous (BAM image not shown). At ~15 mN/m the first bright spots appear which we currently ascribe to the partial crystallization of the monolayer (Fig. 2b). Starting from a pressure of ~32 mN/m up to a pressure of ~35 mN/m the individual areas of the spots grow until they nearly cover the entire subphase at ~37 mN/m (Fig. 2c) [16].

Surface potential measurements suggest that there are no specific interactions between the hydrophilic headgroup of **1** and the Ca ions in the aqueous subphase. The surface potential on water starts to rise at ~190–195 Å^2/molecule and on $CaCl_2$ at ~185–190 Å^2/molecule, where the surface pressure still is at zero. The potential curve shows a steep increase finally reaching ΔV_0 values of about 255 mV on water and 270 mV on $CaCl_2$.

The potential curve of **1** on H_2O shows a second point of inflexion at a surface area of 180 Å^2 which is coincident with the onset of pressure increase in the Langmuir isotherm thus indicating that a homogeneous monolayer has formed at this point. Thereafter, the increase of the potential curve is less steep until at the collapse pressure a limiting surface potential value is reached (ΔV_C=325 mV on H_2O and 340 mV on $CaCl_2$, respectively).

Table 1
Area/molecule of calix[4]arene derivatives as determined from Langmuir isotherms and from crystal data

Compound	Area/molecule [nm^2]		Ref.
	Monolayer (subphase)	Crystal data (compound)	
1	1.70–1.75 (H_2O)[a]	1.44	this work, [13]
	1.70–1.75 ($CaCl_2$)[b]	n.d.	this work
2	1.45–1.50[a]	1.51 (**4**)	[10]
	1.65–1.70[b]	1.70 (**5**)	[10]
3	1.65–1.70[a]	1.60 (**6**)	[11]
	1.75–1.80[b]	1.83 (**7**)	[11]

Compound index: **1**: $C_{68}H_{104}O_8$, **2**: $C_{68}H_{96}O_{12}$, **3**: $C_{68}H_{96}O_{12}$, **4**: $C_{68}H_{96}O_{12}\cdot 4.75CH_3OH\cdot 0.25H_2O$, **5**: $[Ca(C_{68}H_{92}O_{12}Ca)(DMSO)_2(H_2O)]\cdot 2.5DMSO$, **6**: $C_{84}H_{128}O_{16}\cdot (CH_3CN)_{1/8}$, **7**: $[Ca(C_{84}H_{126}O_{16})(DMSO)_2(H_2O)_2]\cdot (DMSO)\cdot (H_2O)_4$.
n.d.=not determined.
[a] Double de-ionized water, resistance 18.2 MΩ cm.
[b] Aqueous subphase containing $CaCl_2$, c=10 mM.

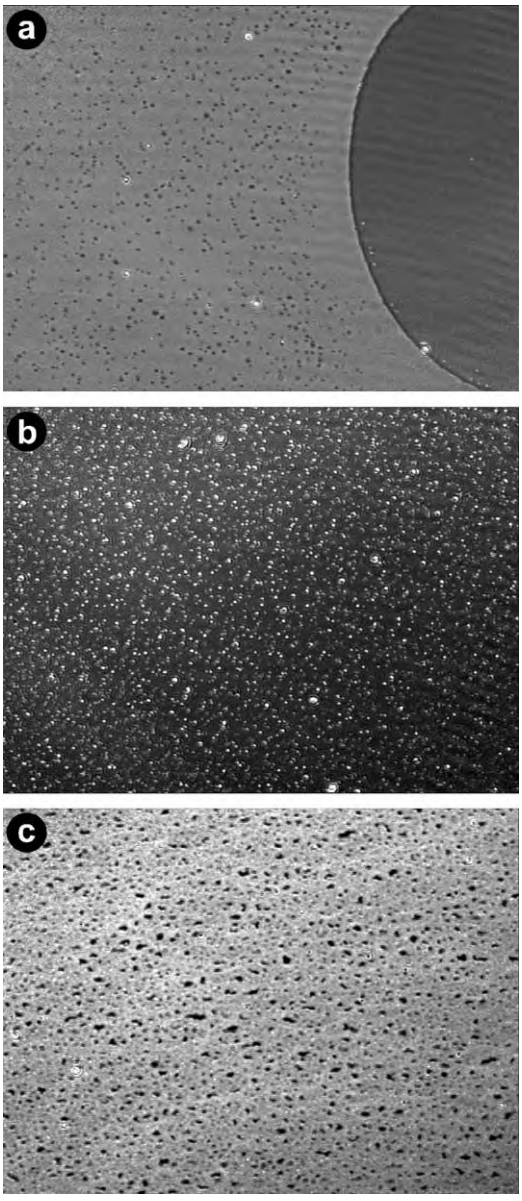

Fig. 2. BAM micrographs of monolayers of **1** on 10 mM $CaCl_2$ at 22 °C. Monolayer domains appear as light regions. Image (a) was recorded at zero surface pressure, image (b) at 32 mN/m, and image (c) at 37 mN/m. Size: 430×320 μm^2.

Previously reported details on the monolayer characteristics of compound **2** are augmented here by surface potential measurements [10]. The π–A isotherm recorded from spreading **2** on a 10 mM $CaCl_2$ subphase (Fig. 1, bottom) shows a pronounced expansion effect, i.e. the mean molecular area of **2** is by 12% larger than the corresponding value from the isotherm data of **2** on pure water. This behaviour is obviously due to electrostatic/coordinative interactions between Ca ions and the deprotonated carboxylic acid residues. Remarkably, the expansion effect is also observed in the supramolecular packing of **2** if the crystal structures of the free acid and its Ca complex are compared with each other (Table 1) [10].

The surface potential of **2** on water starts to rise at ~155–160 $Å^2$/molecule and on $CaCl_2$ at ~180 $Å^2$/molecule, where the surface pressure still is at zero (Fig. 1). The potential curves show a steep increase up to ΔV_0 values of about 200 mV on water and 490 mV on $CaCl_2$, respectively. After the first point of inflexion the increase of the potential curve is less steep until the final potential values are reached (ΔV_C=310 mV on H_2O and 775 mV on $CaCl_2$) and the Langmuir isotherms indicate that the monolayers collapse.

Two facts deserve special attention if the monolayers are compared to each other. First, it should be noticed that the surface potential curves of **1** and **2** on H_2O are virtually identical. The final surface potential values ΔV_C at the collapse point differ by only 15 mV which is within the experimental error (ca. ±15 mV) of the surface potential measurements. In contrast, the ΔV_0 value of **1** is about 55 mV higher than that of **2** (H_2O subphase). A similar trend is observed for the monolayer data of the stearyl alcohol and stearic acid, respectively [17], which demonstrates that at the air–water interface, amphiphilic cone-shaped calix[4]arenes such as **1** and **2** behave similar to simple monofunctional surfactants.

Second, a major difference between monolayers of **1** and **2** arises on aqueous subphases containing Ca ions. While the potential curve of **1** on 10 mM $CaCl_2$ indicates no interaction between the monolayer and the ions from the aqueous subphase, the diagram of **2** (Fig. 1) shows a huge jump of the surface potential: ΔV_C of **1** is 340 mV (10 mM $CaCl_2$) whereas ΔV_C of **2** amounts to 775 mV (10 mM $CaCl_2$), which is 465 mV higher than ΔV_C on H_2O. For comparison: the surface potential of stearic acid at collapse pressure is 345 mV (10 mM $CaCl_2$), as opposed to 285 mV (H_2O). The huge shift of the ΔV_C value of **2** on a Ca-containing subphase most likely attributes to the strong Ca affinity of **2**. Previous structural investigations have in fact shown that the octadentate ligand **2** readily forms a mononuclear Ca complex [10]. In this regard the amphiphilic calix[4]arene **2** behaves dissimilar to monofunctional surfactants where the low Ca affinity leads to formation of a diffuse adlayer of Ca ions underneath the monolayer. (Recent grazing incidence X-ray diffraction experiments of arachidate monolayers indicate that, on average, only one Ca ion is bound per 4–8 surfactant molecules [8].)

We conclude that formation of a Ca complex of **2** gives rise to a huge increase of surface potential which is not observed for the electrostatically neutral compound **1**. Upon compression the cone-shaped calix[4]arenes **1** and **2** both show an increase in surface potential indicative of a pressure-dependent co-orientation of molecular dipoles at the air–water interface. This behaviour once again is reminiscent to the monolayer properties of simple monofunctional surfactants which shows that amphiphilic calix[4]arenes can be regarded as stiff molecular dipoles (the vector of the molecular dipole moment coincides with the pseudo C_{4v} symmetry axis of the molecule). The Langmuir isotherms of **1** and **2** furthermore show that, at the onset of

pressure, both monolayers are in a liquid-expanded state where the arrangement of molecules is lacking a long-range order [10]. Whereas the monolayers of **2** do not show any indication of a phase transition until film collapse occurs, the phase behaviour of **1** at a pressure >5 mN/m is more complex and the BAM investigations hint at formation of a highly ordered liquid condensed phase. GIXD investigations are currently underway to prove this assumption.

2.2. $CaCO_3$ crystallization underneath monolayers

Crystal growth was observed in situ by optical microscopy (Fig. 3). The orientation of calcite crystals was determined by X-ray powder diffraction and geometrical analysis. A more detailed description of the procedure is given elsewhere [10].

Upon spreading monolayers of **1** on a 9 mM $Ca(HCO_3)_2$ we observe a marked inhibition of $CaCO_3$ crystal nucleation. The calcite single crystals which grow underneath monolayers of **1** most often possess the highly symmetrical shape of the calcite {10.4} cleavage rhombohedron. A quantitative analysis of optical micrographs of $CaCO_3$ crystals grown underneath monolayers of **1**, or at the air–water interface (without monolayer), respectively, reveals a strong inhibition effect: the crystal density observed underneath monolayer of **1** is roughly 0.1 times that of the control experiment. Monolayers of stearyl alcohol or cholesterol show similar inhibition effects [18]. It is conceivable that the octadentate calix[4]arene derivative **1** might sequester a single Ca ion in a fashion similar to the carboxylic acid derivative **2**. Based on the surface potential measurements presented here, however, this assumption can be ruled out.

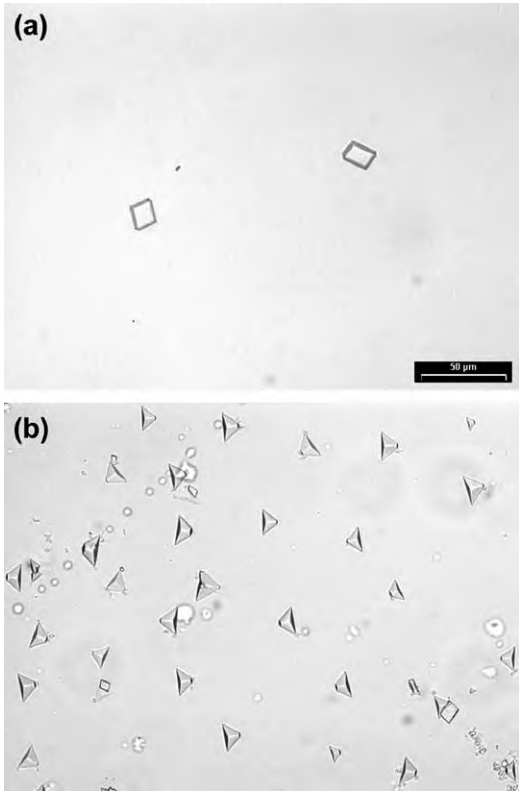

Fig. 3. Optical micrographs of calcite single crystals grown under a monolayer of **1** and **2** on $CaCl_2/NaHCO_3$ (c=9/18 mM) after 6 h (π=0.1 mN/m).

In contrast to the inhibition effect of **1**, uniformly oriented calcite single crystals form underneath monolayers of **2** at low surface pressure (π=0.1–0.5 mN/m). The calcite single crystals obtained display the typical shape of truncated rhombohedrons (Fig. 3b). The truncation occurs parallel to the {01.2} faces of the calcite crystal lattice [10]. The $CaCO_3$ crystal density underneath the monolayer of **2** is approximately 20 times that of the density underneath monolayers of **1** under the same experimental conditions and the spacing between different calcite crystals which attach to the monolayer is highly regular. These observations indicate that monolayers of **2** at low surface pressure (π=0.1–0.5 mN/m) direct nucleation and growth of calcite crystals while underneath monolayers of **1** crystal growth becomes inhibited. At higher surface pressure (π=5–25 mN/m) non-truncated calcite rhombohedra form which lack any preferential orientation. The nucleation density at high surface pressure is reduced (approximately 1/5) and the spacing between different calcite crystals attached to the monolayer is much less regular as compared to the monolayer of **2** at low surface pressure.

2.3. Concluding remarks

In this study we have examined electrostatic interactions between monolayers of structurally related amphiphilic calix[4]arene derivatives **1** and **2** and subphase ions by employing surface potential measurements. In the low pressure region (π=0.0–0.5 mN/m) of the monolayer phase diagram the experimental ΔV_0 values for monolayers of **1** and **2** on H_2O are almost identical. On a Ca-containing subphase (10 mM $CaCl_2$) ΔV_0 shows a significant increase only for monolayers of **2** which clearly demonstrates that calix[4]arene derivative **1** is unable to bind Ca ions by virtue of electrostatic and/or coordinative interactions.

Our experiments furthermore indicate that a low surface pressure (π=0.1–0.5 mN/m) is a necessary condition for the growth of uniformly oriented calcite crystals [19]. The phase diagram of **2** and previous studies on the monolayer structure [10] show no indication of long range order in the monolayer, that is the x- any y-components of the molecular dipole moments are laterally uncorrelated.

The templating role of monolayers has frequently been interpreted in terms of a geometrical and stereochemical complementarity between the arrangement of headgroups in the monolayer and the position of Ca ions in the crystal plane which attaches to the monolayer [2–7,20].

Our investigations, however, demonstrate that such delicate and complex interactions most likely vanish if structurally mobile template matrices such as monolayers

are employed. Most probably non-specific electrostatic effects such as the average charge density or the mean dipole moment of the monolayer determine the orientation of crystals [5,21]. In fact in all of our investigations conducted so far, the growth of (01.2) oriented calcite crystals occurred at a surface area corresponding to 1.70–1.80 nm^2/molecule which leads to an average density of 2.22–2.35 carboxylate residues/nm^2 [22]. This hypothesis is further supported by our recent investigations on calcium carbonate growth underneath monolayers of *rccc*-4,6,10,12,16,18,22,24-octa-*O*-(carboxymethyl)-2,8,14,20-tetra(*n*-undecyl)resorc[4]arene (**4**), where a change in the number of coordinating residues per molecule from four to eight corresponding to 4.71–5.00 carboxylate residues/nm^2 leads to a completely different $CaCO_3$ growth characteristics (vide infra) [23].

Future investigations will focus on crystallization on $CaCO_3$ underneath mixed monolayers of compounds **1** and **2**. By inserting a nucleation active oligoacid in a matrix of a structurally similar alcohol which inhibits crystal growth, we should be able to explore the lower limit of the charge density which still leads to formation of uniformly oriented calcite single crystals. A further attractive but rather demanding research target concerns the question as to whether or not a *single* molecule of an oligoacid can promote formation of a single $CaCO_3$ crystal nucleus. Structurally well-defined oligomeric acids such as **2** or **3** might turn out to be valuable model compounds in this regard.

3. Experimental

Melting points were determined with an electrothermal melting point apparatus and were uncorrected. FT-IR spectra were recorded from KBr pellets on a Shimadzu FTIR-8300 spectrometer. ^1H and ^{13}C NMR spectra were recorded on a Bruker DRX 500 spectrometer in $CDCl_3$ at room temperature with residual solvent. Elemental analysis was carried out with a Perkin-Elmer 240 elemental analyzer. All reagents were reagent grade and used without further purification.

4. 5,11,17,23-Tetrakis-(1,1,3,3-tetramethylbutyl)-25,26,27,28-tetra(2-hydroxyethoxy)calix[4]arene (1)

The product was prepared according to a slightly modified procedure [24]. To a stirred suspension of $LiAlH_4$ (1.3 molar excess with respect to the corresponding stoichiometric ratio) in 10 mL of dry THF was added dropwise a solution of 5,11,17,23-tetrakis-(1,1,3,3-tetramethylbutyl)-25,26,27,28-tetra(ethoxycarbonylmethoxy)calix[4]arene (250 mg, 0.21 mmol) in 10 mL dry THF. The reaction mixture was stirred for 12 h under an argon stream. The excess of $LiAlH_4$ was destroyed by careful addition of water and the solvent was evaporated under reduced pressure. The residue was diluted in chloroform and washed with sulphuric acid (3×30 mL, 10%) and water (3×30 mL). The organic phase was evaporated under reduced pressure and the crude product was recrystallized from ethanol to give the desired product as crystalline solid. Mp. 240 °C (ethanol).

IR (cm^{-1}): $\tilde{\nu}$ 3462, 2952, 1601, 1475, 1366, 1250, 1205, 1085, 1047, 866, 806.

^1H NMR (500 MHz, 25 °C, TMS): δ=6.80 (s, 8 H, ArH), 5.10 (s, 4 H, OH), 4.33 (d, ^2J=12.6 Hz, 4 H, $ArCH_2$), 3.97 (m, 8 H, OCH_2CH_2, 3.93 (m, 8 H, OCH_2CH_2) 3.19 (d, ^2J=12.7 Hz, 4 H, Ar-CH_2), 1.51 (s, 8 H, CCH_2C), 1.09 (s, 24 H, CH_3), 0.65 (s, 36 H, CH_3). ^{13}C NMR (125 MHz) δ=152.4 (Ar 25,26,27,28-C), 145.0 (Ar 5,11,17,23-C), 133.2 (Ar 1,3,7,9,13,15,19,21-C), 126.3 (all ArC-H), 77.9 ($ArOCH_2CH_2OH$), 61.7 ($ArOCH_2CH_2OH$), 57.3 (CCH_2C), 37.9 (Ar-CCH_2), 32.3 (CH_2C), 31.6 ($ArC(CH_3)_2$), 31.1 ($CH_2C(CH_3)_2$), 30.6 ($ArCH_2Ar$). Elemental analysis calcd. for $C_{68}H_{104}O_8$: C 77.82, H 9.99; found: C 77.11, H 9.33.

5. 5,11,17,23-Tetrakis-(1,1,3,3-tetramethylbutyl)-25,26,27,28-tetra(carboxymethoxy)calix[4]arene (2)

Compound **2** was synthesized according to the procedure described in a previous paper [10].

5.1. Monolayer investigations

Monolayer experiments were performed with a double-barrier NIMA trough using a compression speed of 15 cm^2/min in order to ensure reproducibility. The surface pressure of the monolayers was measured using a Wilhelmy plate. Langmuir monolayers were formed on aqueous subphases by spreading compound **1** from a trichloromethane/methanol (9:1) solution (50 µl, 0.5 mg/mL) and **2** from a trichloromethane solution (50 µl, 0.5 mg/mL). Compression was started after 10 min. Simultaneously, the surface potential was recorded using a vibrating plate located at ca. 2 mm above the water surface. The reference electrode, made from stainless steel, was placed in the aqueous subphase. Each isotherm was measured at least three times. Brewster angle microscopy were performed with a NIMA Langmuir trough (NIMA 601BAM) using a BAM-2 (NFT, Göttingen).

5.2. $CaCO_3$ crystal growth experiments

Solutions of calcium bicarbonate were prepared by bubbling carbon dioxide gas through a stirred aqueous (double de-ionized H_2O, resistance 18.2 MΩ cm) solution of $CaCl_2/NaHCO_3$ (c=9/18 mM) for a period of 2 h. Compressed films were formed by spreading the solutions of surfactants in order to generate liquid-like films at the air–water interface. Crystals were studied after several times either in situ by optical microscopy (PZO Biolar upright

microscope) or on cover slips laid on the film (Olympus IX70). Crystal growth experiments were repeated at least five times.

Crystallographic indices are presented in three-index (*hk.l*) notation, based on the hexagonal setting of the calcite unit cell ($R\bar{3}c$, a=4.96 Å, c=17.002 Å).

Acknowledgements

D.V. thanks the DFG for a Habilitanden fellowship. M.F. thanks the Graduiertenförderung Nordrhein-Westfalen for a graduate fellowship. This work was financially supported by the Deutsche Forschungsgemeinschaft (DFG Schwerpunktprogramm 1117, “Prinzipien der Biomineralisation”; DFG grant Vo829/2). Donation of the starting material *p*-1,1,3,3-tetramethylbutylphenol by CONDEA Chemie GmbH (Marl, Germany) is gratefully acknowledged.

References

[1] a H.A. Lowenstam, S. Weiner, On Biomineralization, Oxford University Press, Oxford, 1989;
b S. Mann, Biomineralization. Principles and Concepts in Bioinorganic Materials Chemistry, Oxford University Press, Oxford, 2001.
[2] a S. Mann, B.R. Heywood, S. Rajam, J.D. Birchall, Nature 334 (1988) 692;
b S. Champ, J.A. Dickinson, P.S. Fallon, B.R. Heywood, M. Mascal, Angew. Chem., Int. Ed. Engl. 39 (2000) 2716;
c P.J.J.A. Buijnsters, J.J.J.M. Donners, S.J. Hill, B.R. Heywood, R.J.M. Nolte, B. Zwanenburg, N.A.J.M. Sommerdijk, Langmuir 17 (2001) 3623.
[3] a J. Aizenberg, A.J. Black, G.M. Whitesides, Nature 398 (1999) 495;
b J. Küther, G. Nelles, R. Seshadri, M. Schaub, H.J. Butt, W. Tremel, Chem. Eur. J. 4 (1998) 1834;
c D.D. Archibald, S.B. Qadri, B.P. Gaber, Langmuir 12 (1996) 538.
[4] a A. Berman, D.J. Ahn, A. Lio, M. Salmeron, A. Reichert, D. Charych, Science 269 (1995) 515;
b H. Cölfen, M. Antonietti, Langmuir 14 (1998) 582.
[5] a L. Addadi, J. Moradian, E. Shay, N.G. Maroudas, S. Weiner, Proc. Natl. Acad. Sci. U. S. A. 84 (1987) 2732;
b S.R. Letellier, M.J. Lochhead, A.A. Campbell, V. Vogel, Biochim. Biophys. Acta 1380 (1998) 31.
[6] S. Mann, D.D. Archibald, J.M. Didymus, T. Douglas, B.R. Heywood, F.C. Meldrum, N.J. Reeves, Science 261 (1993) 1286.
[7] a L. Addadi, S. Weiner, in: S. Mann (Ed.), Biomineralization, VCH, Weinheim, 1989, pp. 133–156;
b J. Aizenberg, A.J. Black, G.M. Whitesides, J. Am. Chem. Soc. 121 (1999) 4500.
[8] E. DiMasi, M.J. Oltsza, V.M. Patel, L. Gower, CrystEngComm 5 (2003) 346.
[9] M.J. Lochhead, S.R. Letellier, V. Vogel, J. Phys. Chem., B 101 (1997) 10821.
[10] D. Volkmer, M. Fricke, D. Vollhardt, S. Siegel, J. Chem. Soc., Dalton Trans. (2002) 4547.
[11] D. Volkmer, M. Fricke, C. Agena, J. Mattay, CrystEngComm 4 (2002) 288.
[12] a D.M. Taylor, Adv. Colloid Interface Sci. 87 (2000) 183;
b P. Dynarowicz-Latka, A. Dhanabalan, O.N. Oliveira Jr., Adv. Colloid Interface Sci. 91 (2001) 221.
[13] Crystal data of **1**: monoclinic, space group $C2/c$; Z=4, a=25.8237(13), b=12.2123(6), c=21.1292(10) Å; β=108.715(1)°. Details on the crystal structure will be reported elsewhere.
[14] K. Ichimura, M. Fujimaki, Y. Matsuzawa, Y. Hayashi, M. Nakagawa, Mater. Sci. Eng., C 8–9 (1999) 353.
[15] P. Dynarowicz-Latka, A. Dhanabalan, A. Cavalli, O.N. Oliveira Jr., J. Phys. Chem. 104 (2000) 1701.
[16] W. He, D. Vollhardt, R. Rudert, L. Zhu, J. Li, Langmuir 19 (2003) 385.
[17] The ΔV_C value of a stearyl alcohol monolayer on H_2O (400 mV) is 115 mV higher than that of a stearic acid monolayer (285 mV). a) O.N. Oliveira, Jr., C. Bonardi, Langmuir 13 (1997) 5920; b) V. Vogel, Struktur und Dynamische Eigenschaften von Monomolekularen Lipidfilmen, PhD Thesis, Johann Wolfgang Goethe Universität, Frankfurt, 1987.
[18] S. Rajam, B.R. Heywood, J.B.A. Walker, S. Mann, R.J. Davey, J.D. Birchall, J. Chem. Soc., Faraday Trans. 87 (1991) 727.
[19] S.J. Cooper, R.B. Sessions, S.D. Lubetkin, J. Am. Chem. Soc. 120 (1998) 2090.
[20] a B.R. Heywood, S. Mann, Chem. Mater 6 (1994) 311;
b I. Weissbuch, M. Lahav, L. Leiserowitz, Cryst. Growth Des. 3 (2003) 125.
[21] P. Calvert, S. Mann, Nature 386 (1997) 127.
[22] D. Volkmer, M. Fricke, Z. Anorg. Allg. Chem. 626 (2003) 2381.
[23] D. Volkmer, M. Fricke, C. Agena, J. Mattay, J. Mater. Chem. 14 (2004) 2249.
[24] S.E. Matthews, P. Schmitt, V. Felix, M.G.B. Drew, P.D. Beer, J. Am. Chem. Soc. 124 (2002) 1341.